A Finite Element Model for Mechanical Analysis of LHC Main Dipole Magnet Coils

Mirko Pojer, Arnaud Devred and Walter Scandale

***Abstract*— After years of studies and observations, the mechanical stability of the LHC main dipole magnets still remains an open issue. The robustness of these magnets has already been asserted and their reliability in operation is not far from being proven. However, anomalous mechanical behaviors sometimes observed are not yet completely understood. A finite element model, which has been recently developed at CERN, aims at providing an instrument for better explaining these anomalies. Cable modeling and contact between elements, friction and mechanical hysteresis are the key features of this model. The simulation of the hysteresis experienced by the coil during collaring, presented here, is the starting point for the representation of the whole life cycle of the dipole coil.**

***Index Terms*— Finite element model, LHC, superconducting accelerator magnet, mechanical hysteresis.**

I. Introduction

After nearly two decades, many papers have been written on the Large Hadron Collider [1], presently under construction at CERN, Geneva. The production of the 1232 arc dipole magnets is near completion and the cold testing of these important elements will be over before the end of the year. They have fulfilled all the requirements [2] and the operation reliability of these magnets is close to being confirmed.

From an academic standpoint, nevertheless, the anomalous mechanical behaviors, which were sometimes observed during power tests, have not yet been given a clear explanation. The work presented in this paper aims at providing an instrument to better understand the reasons for such anomalies, by means of finite element modeling of the cross-section of the dipole coil. The elaboration of this model has already been introduced elsewhere by the same authors [3] and all the pattern details are only briefly recalled here. In this paper, we focus on the important role of friction and on how to reproduce the hysteretic behavior exhibited by the magnet coil upon loading/unloading, as in the case of collaring of the magnet. The modeling of such behavior is a novelty in this kind of application.

Manuscript received August 28, 2006.

This work was supported in part by the Ecole Polytechnique Fédérale de Lausanne – Programme Doctoral en Physique.

Mirko Pojer is with CERN, Accelerator Technology Department, CH-1211 Geneva 23, Switzerland and Ecole Polytechnique Fédérale de Lausanne – Programme Doctoral en Physique (phone: +41-22-767378; fax: +41-22-7676300; e-mail: mirko.pojer@cern.ch).

Arnaud Devred is with CEA/Saclay, DSM/DAPNIA/SACM, 91191 Gif-sur-Yvette, CEDEX France and CERN, Accelerator Technology Department, CH-1211 Geneva 23, Switzerland (e-mail: arnaud.devred@cern.ch).

Walter Scandale is with CERN, Accelerator Technology Department, CH-1211 Geneva 23, Switzerland (e-mail: walter.scandale@cern.ch).

II. Objectives and Definition of the Model

It has been clearly illustrated how important is a good positioning of the cables in a magnet cross-section and which is the fundamental role of azimuthal pre-stress [4]. There are numerous studies of the consequences of conductor motion under the effect of electro-magnetic forces and of the loss of pre-stress during energization [5]. However, no model has ever been able to reproduce in detail and predict such phenomena.

The present model, developed in ANSYS® environment, was initiated with the idea of representing the real behavior of an LHC-type dipole coil, by taking into account each turn individually, reproducing the non-linear and hysteretic mechanical behavior observed on a stack of insulated cables [6] and inserting friction between mating surfaces.

To prove the feasibility of such kind of model, we aimed at reconstructing the experimental setup for the elastic modulus measurements on single layers (both inner and outer) and on poles, which are performed in industry; actually, these are the only relevant experimental results at our disposal.

Limiting the model to the straight part of the coil and being only interested in the coil itself, the model can be restricted to a quarter of a magnet aperture, as illustrated in Fig.1. As such, it reproduces exactly the configuration for Young's modulus measurements at the manufacturers' premises, where the upper mould is pressing the two coil layers, with the inter-layer spacer in between.

A detailed description of the model can be found in [3]. Let us just mention here that, differently from previous models [7], the two layers are not bonded together and the inter-layer spacer is added in the modeling. The choice of starting from separated layers is imposed by the necessity of limiting initial interference. Concerning the material properties, as explained in [3], we rely on quadrilaterals with homogeneous material properties (insulation included) to model the cables, whereas the insulated copper wedges are divided into four sectors with orthotropic elastic modulus. Regarding the cable, it was as well mentioned that the Young's modulus should be taken as orthotropic; nevertheless, simulations, performed using a Young's modulus different for radial and azimuthal directions, have proven that this split has

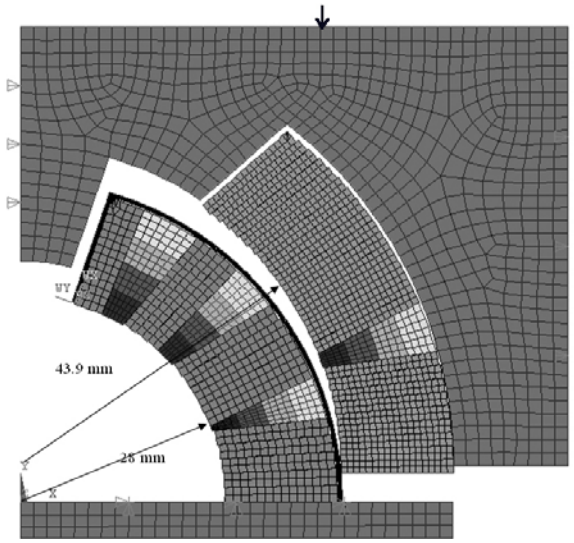

Fig. 1. Finite element model of a half pole during Young's modulus measurements.

little effect on the results. Hence the elastic modulus has been set as isotropic.

It was also explained in our previous paper that the nominal geometry is defined for an applied stress of 40 MPa. The zero-load dimensions of the cables have been determined (see Table I), assuming thicker and less wide quadrilaterals, and used in the model to define the zero-load starting configuration. Due to their stiffness, the copper wedges do not need to be re-dimensioned.

TABLE I
LOADED VS UNLOADED CABLE DIMENSIONS

	Inner layer		Outer layer	
	40 MPa	zero-load	40 MPa	zero-load
Thin edge [mm]	1.973	1.973+0.042	1.62	1.62+0.024
Thick edge [mm]	2.307	2.307+0.052	1.86	1.86+0.028
Width [mm]	15.40	15.40-0.060	15.40	15.40-0.038

III. NEW DEVELOPMENTS

A. Contact Characterization

Two types of contact are used in the model: surface-to-surface (CONTA172-TARGE169) and node-to-surface (CONTA175-TARGE169) contact elements. Considering all possible combinations between mating surfaces, the total number of contact pairs is 118, while there are 15 different contact types. Each type of contact is characterized by 5 parameters: the normal and transverse contact stiffness, the allowable penetration, the slipping factor and the friction. The resulting 75 free parameters have been reduced or adjusted by imposing some boundary conditions:

- the maximum penetration is set to 1 μm when dealing with soft materials, a larger value is used when excessive penetration is already prevented by the material's rigidity (the ideal case would be to put all penetrations to zero, but this is too time-consuming from the point of view of mathematical convergence, or not solvable at all);
- the normal stiffness is initially set to 1 and progressively increased in case of excessive penetration;
- the friction coefficients for cable-to-cable contacts are set to larger values than for the other contacts, to simulate the fact that, in practice, the insulated coil turns are glued as the result of curing.

In most cases, mathematical convergence has been privileged, being nevertheless respectful of the physical sense of selected values.

A thorough analysis has been performed, to study the influence of the parameters on the accuracy with which the model can represent the available measurements, and sensitivity tables have been built. All coefficients, but the friction ones, are found to strongly influence the convergence but to have little effects on the result. As foreseeable, the friction coefficients have been found to be most relevant for result precision. A summary of the selected friction coefficients can be found in Table II.

TABLE II
FRICTION COEFFICIENTS (μ) SELECTED FOR THE DIFFERENT CONTACT TYPES

Contact pair	μ	Contact pair	μ	Contact pair	μ
cab. in/cab. in	0.8	cab. in/mould	0.4	Cu-wed. out/int.sp.	0.2
cab. in/Cu-wed.	0.4	int.sp./mould	0.1	last cab. out/mould	0.4
cab. in/int.sp.	0.2	cab. out/cab. out	0.8	1st cab. out/mould	0.4
Cu-wed. in/int.sp.	0.2	cab. out/Cu-wed.	0.4	cab. out/mould	0.6
last cab. in/int.sp.	0.2	cab. out/int.sp.	0.2	Cu-wed. out/mould	0.4

Abbreviations: cab.=cable; Cu-wed.=copper wedge; int.sp.=inter-layer spacer.

B. Unloading of the Structure

To represent the piece-wise linear elastic properties of insulated cables, the Multilinear ELAStic function (MELAS) is used. It has important limitations. First of all, in principle, it can only account for the behavior of elastically isotropic materials; this is only partially true, in the sense that we proved that the relation is still valid between the maximum elastic moduli in two orthogonal directions and the relative Poisson ratios, even when dealing with a function exclusively defined for isotropic materials:

$$E_{x,\max} \Big/ E_{y,\max} = \nu_{xy} \Big/ \nu_{yx} \tag{1}$$

where E_i is the Young's modulus in the i-direction and ν_{ij} is the Poisson's ratio from the i- to j- direction.

Changing the Poisson's ratio relative to one direction, we can change the corresponding stiffness. As mentioned before, however, this was not necessary, since the orthotropic nature of the insulated cables was proven to have little influence on the simulation results.

Another limitation comes from the fact that the MELAS function only describes a conservative (path-independent) response: no hysteresis can be represented by this function. In fact, even if we can include friction in the MELAS parameters, this does not account for the real dissipative phenomena.

To circumvent this difficulty, we have chosen to represent the loading and unloading branches with different material curves, and to reconstruct the unloading part with a non unique curve, depending on the maximum stress level reached

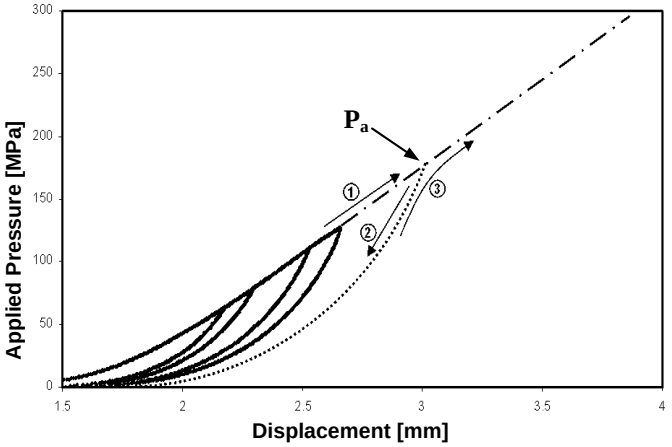

Fig. 2. Summary of the procedure followed to represent the unloading phase for an element reaching a pressure P_a: 1-extrapolation of the existing data to larger values; 2- application of the unloading fit (2); 3- junction of unloading and loading curves, in case of further increase of applied pressure.

during loading. After trials, we have decided to use a single loading and 36 different unloading paths, discretized in 10 MPa steps, so as to simulate local stress concentration points with a Von Mises stress value up to 360-400 MPa, when the applied stress reaches 160-180 MPa.

Since the stress-strain characteristics were measured only up to 100-120 MPa [8], one necessary step needed for the hysteresis reconstruction has been the extrapolation of the ramp-up data to 400 MPa; if we assume to always work in the elastic regime, we can linearly extend the upper straight part of the stress-strain curve.

To build the unloading curves, we have deduced a scaling law from the few unloading curves that were measured. After several attempts, a coherent and simple common fit for these curves has been found in the form of:

$$\Delta = \left(k_1 \cdot P_{\max} + k_2\right) \cdot P^{\left(k_3 \cdot P_{\max} + k_4\right)} - \left(k_5 \cdot P_{\max} + k_6\right) \qquad (2)$$

where Δ is the reduction in stack height under pressure P, P_{max} is the maximum applied stress during loading and $k_1 \div k_6$ are constant coefficients. The trend that better represents each curve is a power law for the pressure, and the structure of the $(k_n \cdot P_{max} + k_{n+1})$ terms has been chosen according to their necessity of being maximum-stress-dependent. Solving the 6-parameters fit by minimizing the squared sum of all the residuals (data minus fit), we got in reality a k_3 value close to zero, which means that the power law exponent is maximum-stress independent.

Fig. 2 illustrates the procedure followed for a single element (the solid curves are the measured stress-displacement characteristics, for both loading and unloading):

- for applied stress, P_a, above the maximum stress value achieved in the measurements, we extrapolate along the solid-dotted curve (part 1);
- applying the fit, we reconstruct the dotted-lined unloading branch (part 2);
- if the pressure is increased again after ramp down, the new loading path would be represented by the unloading branch plus the upper part of the original loading curve, following path 3.

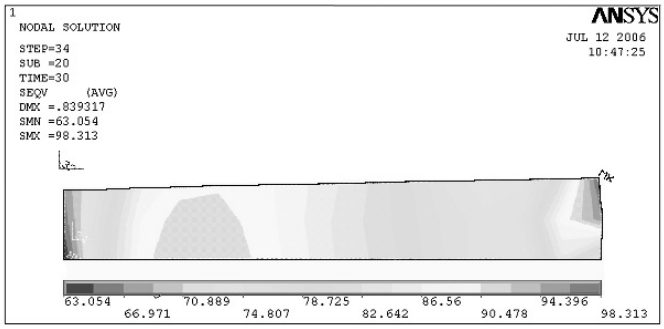

Fig. 3. Stress distribution in one of the cables of the inner layer, after applying a 100 MPa load to the whole layer.

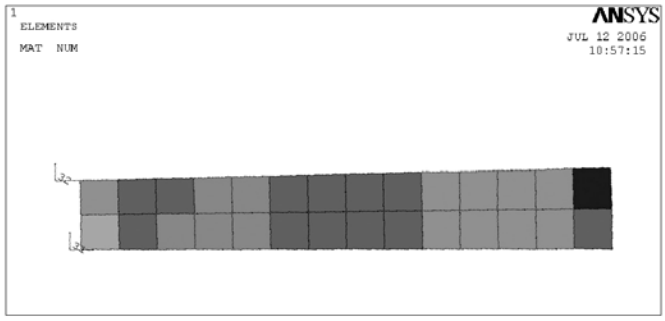

Fig. 4. Result of the application of the MPCHG function to the cable of Fig. 3, featuring 5 different materials to represent the previously homogeneous cable.

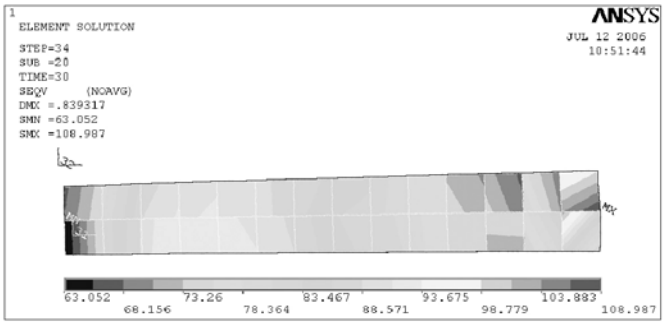

Fig. 5. New Von Mises stress map after the application of the MPCHG function. The structure is ready for unloading.

The change in material properties is done using the function MPCHG (change of material number attributes): all the elements with a stress value between *x* and *x+10* MPa are selected and the unloading curve corresponding to a peak stress of *x+10* MPa is attributed to them. This discretization imposes that all the points on the loading curve have to be shifted to the right on the chart, to cross the nearest unloading curve; and due to the fact that the stress distribution must remain the same, the shifts result in an increase of the geometrical compression for every element, with a maximum for the elements having the lowest stress values in a certain range (and being the furthest away from the corresponding unloading curve). This is at the origin of the necessity of fine-segmenting the unloading part.

In Figs. 3 to 5, the use of the MPCHG function is illustrated, as applied to a cable with a high stress gradient: after loading the structure with an external pressure of 100 MPa, different stress values can be observed along the

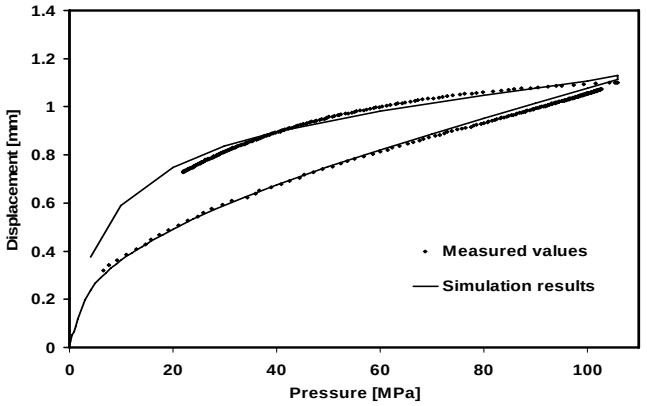

Fig. 6. Loading-unloading cycle for the outer layer. Model results are compared with measured values.

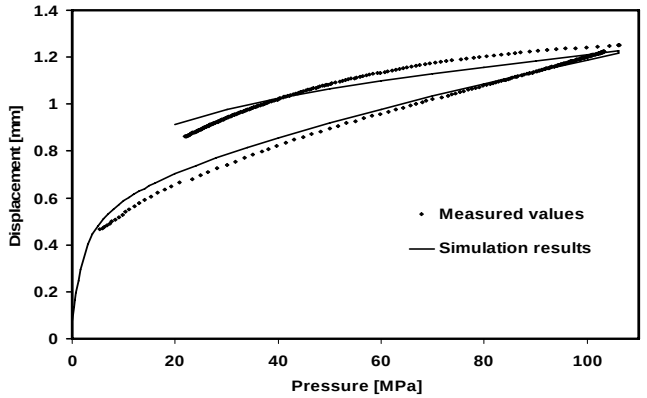

Fig. 7. Loading-unloading cycle for the inner layer. Model results are compared with measured values.

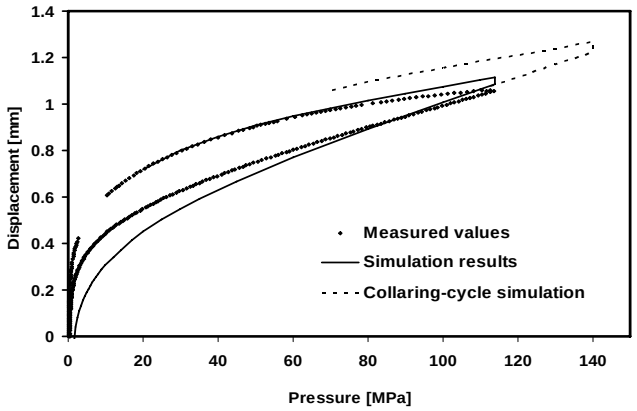

Fig. 8. Hysteretic cycle for the pole. The dotted line represents the ideal collaring, with an increase of the pressure up to 140 MPa and the spring-back.

cable width (Fig. 3); four decades in stress amplitude give rise to an equivalent number of material categories in the cable, as shown with different gradations in Fig. 4. Comparing Figs. 3 and 5, it appears that the resulting Von Mises stress distribution does not change considerably from the original figure, and that the extreme stress values are only 10 % higher.

IV. Results

The outcome of the application of the procedure we have just described is the reconstruction of the elastic modulus measurements, performed in industry on single layers and on assembled poles. In Figs. 6 and 7, the comparison between representative experimental measurements and the simulation results is presented, for both layers.

The hysteresis, typical of the insulated cables, is very well represented, especially for the outer layer, where the discrepancy is very small. It is important to notice that the material change at maximum pressure is responsible for a small additional compression of the structure, as mentioned before; this is in any case almost negligible in both cases.

In the case of the assembled pole (Fig. 8), the resemblance of measured and simulated values is not as good as in the case of single layers, but it is nevertheless satisfactory. We reduced the difference from that reported in [3] to less than 10%, and this is a great improvement, especially in relation with the analytical calculation, which was overestimating the Young's modulus of the pole by 50%. The dotted line in Fig. 8 represents the ideal collaring cycle, which includes a loading up to nearly 140 MPa and the spring-back effect, responsible for the unloading down to around 70 MPa.

This may be considered as the starting point for the reproduction of the whole life-cycle of a magnet coil, the following steps being the cooling of the structure and the application of a Lorentz forces map.

V. Conclusion

The hysteretic behavior exhibited by the magnet coil upon loading/unloading has been presented. This is the result of a complex modeling, which takes into account the fine structure of the coil and introduces friction between mating components. The collaring cycle of the coil has been modeled; this is the first step in a simulation of the whole life-cycle of the coil.

Acknowledgment

The authors wish to thank A. Wrulich, L. Rivkin (PSI-Villigen/EPFL), J.-P. Koutchouk and L. Rossi (CERN) for their support.

References

[1] CERN, "LHC Design Report – VOL.1 The LHC main ring", CERN-2004-003, Geneva, June 2004.

[2] A. Siemko et al., "Quench Performance and Field Quality of the LHC Preseries Superconducting Dipoles" , *IEEE Trans. Appl. Supercond.*: Vol. 14, no 2, pp 165-168, 2004.

[3] M. Pojer, A. Devred and W. Scandale, "A Non-linear Finite Element Model for the LHC Main Dipole Coil Cross-section", *IEEE Trans. Appl. Supercond.*: Vol. 16, no 2, pp 1294-1297, 2006.

[4] L. Rossi, "Superconducting magnets for the LHC main lattice", *IEEE Trans. Appl. Supercond.*: Vol. 14, no, 2 pp 153-158, 2004.

[5] P. Ferracin et al., "Modelization of the Thermo-mechanical Structure of the LHC Main Dipole and Influence on Field Quality", *Proceedings of EPAC 2000*, Vienna, Austria, 26-30 Jun 2000.

[6] P. Védrine, B. Gallet and C. Nouvel, "Measurement of thermo-mechanical properties of NbTi windings for accelerator magnets". *IEEE Trans. on Applied Superconductivity*,Vol. 9, no 2, pp 236-239, 1999.

[7] P. Ferracin et al., "Modeling coil pre-stress loss during cool-down in the main dipoles of the LHC", *IEEE Trans. Appl. Supercond.* Vol.12, 2002.

[8] K. Couturier et al., "Thermomechanical properties of the coil of the superconducting magnets for the Large Hadron Collider. *IEEE Trans. on Applied Superconductivity*, Vol.12, no 2, pp 1804-1812, 2002.